High-Energy Electron Scattering and the Charge Distributions of Selected Nuclei*†

BEAT HAHN,‡ D. G. RAVENHALL, AND ROBERT HOFSTADTER
Department of Physics and W. W. Hansen Laboratories of Physics, Stanford University, Stanford, California
(Received October 19, 1955)

Experimental results are presented of electron scattering by Ca, V, Co, In, Sb, Hf, Ta, W, Au, Bi, Th, and U, at 183 Mev and (for some of the elements) at 153 Mev. For those nuclei for which asphericity and inelastic scattering are absent or unimportant, i.e., Ca, V, Co, In, Sb, Au, and Bi, a partial wave analysis of the Dirac equation has been performed in which the nuclei are represented by static, spherically symmetric charge distributions. Smoothed uniform charge distributions have been assumed; these are characterized by a constant charge density in the central region of the nucleus, with a smoothed-out surface. Essentially two parameters can be determined, related to the radius and to the surface thickness. An examination of the Au experiments shows that the functional forms of the surface are not important, and that the charge density in the central regions is probably fairly flat, although it cannot be determined very accurately. An analysis of the experiments on the nuclei Ca, V, Co, In, Sb, Au, and Bi, assuming for convenience the Fermi smoothed uniform shape (1), then leads to the following results: the radial parameter c (the distance to the midpoint of the surface) scales as $A^{\frac{1}{3}}$ for the nuclei we have examined and is $(1.07\pm0.02)A^{\frac{1}{3}}\times10^{-13}$ cm; the surface thickness t (the $0.9\rho_0$ to $0.1\rho_0$ distance) is constant for all of these nuclei, to within the estimated error, and is $(2.4\pm0.3)\times10^{-13}$ cm.

I. INTRODUCTION

IN the last two years several investigations[1–4] have been carried out at Stanford University in an attempt to discover the size and shape of the charge distribution in various atomic nuclei. These investigations have been of an experimental and theoretical nature. The experiments have obtained the angular distributions of high-energy electrons scattered elastically from the atomic nuclei and have employed the narrow momentum selection permitted by the use of a magnetic spectrometer in order to ensure elastic scattering. The theoretical analysis of the experimental observations rests on a phase shift calculation applied to the Dirac equation for a model of the nucleus having a static spherically symmetric charge distribution.[3] Comparisons between the experiments and the theoretical angular distributions for various specialized models of the nuclei have permitted conclusions to be drawn about the size of nuclei, the nuclear charge distribution, and the validity of the assumptions made in the theoretical interpretation. The size obtained from this work, and from the investigations of others,[5–11] has come to be called the "electromagnetic size" in contrast to a "nuclear" size determined from pure nucleon-nuclear interactions. The method of electron scattering is fortunately quite direct in its approach, since its only fundamental untested assumption is that there is no specifically nonelectromagnetic interaction between the scattered electron and the nucleus. Thus far there is no definite evidence of any appreciable deviation of the electron-nucleon interaction from the strict electromagnetic type, so that the foundation on which the theoretical analysis operates seems to be quite secure.

Until the present time the more detailed published data have concerned the heavy nuclei Au^{197} and Pb^{208}. These elements were studied[2] at several different energies in order to test the validity of the theoretical method as applied to a specific nuclear charge-density model. The analysis[4] indicated that two main parameters of the charge distribution could be determined in the present status of the experimental studies extending up to electron energies of 190 Mev. These two parameters may be said to be a mean radius and a surface thickness.

It is the purpose of the present paper to investigate how these two parameters vary over the range of new nuclei studied: Ca, V, Co, In, Sb, Au, and Bi. Another aim of this investigation is to examine, for a specific nucleus, Au, the range of values of the two parameters permitted by a fit of theory to experiment within the experimental errors. Our results for Au and Pb are in agreement with analyses of our earlier experiments by Ravenhall and Yennie,[4] by Brown and Elton,[7] and by Hill *et al.*[8] Furthermore, new experimental data are presented without analysis for nuclei which are probably not intrinsically spherically symmetric in their ground states and which require a more extensive analysis involving their quadrupole moments. Such nuclei as we have studied included Hf, Ta, W, Th, and U.

* The research reported in this document was supported jointly by the Office of Naval Research and the U. S. Atomic Energy Commission, and by the U. S. Air Force through the Office of Scientific Research.
† Aided by a grant from the Research Corporation.
‡ Visiting Research Fellow of the Schweizerische Arbeitsgemeinschaft in Mathematik und Physik.

[1] Hofstadter, Fechter, and McIntyre, Phys. Rev. **92**, 978 (1953).
[2] Hofstadter, Hahn, Knudsen, and McIntyre, Phys. Rev. **95**, 512 (1954).
[3] Yennie, Ravenhall, and Wilson, Phys. Rev. **95**, 500 (1954).
[4] D. G. Ravenhall and D. R. Yennie, Phys. Rev. **96**, 239 (1954).
[5] R. W. Pidd and C. L. Hammer, Phys. Rev. **99** 1396 (1955).
[6] Lyman, Hanson, and Scott, Phys. Rev. **84**, 626 (1951).
[7] G. E. Brown and L. R. B. Elton, Phil. Mag. **46** 164 (1955).
[8] Hill, Freeman, and Ford, Phys. Rev. **99**, 649 (1955)(A).
[9] V. L. Fitch and J. Rainwater, Phys. Rev. **92** 789 (1953).
[10] L. N. Cooper and E. M. Henley, Phys. Rev. **92** 801 (1953).
[11] D. L. Hill and K. W. Ford, Phys. Rev. **94**, 1617 (1954).

II. APPARATUS AND PROCEDURE

The scattering apparatus used in these experiments has been described in earlier papers.[1,2] The following improvements in the apparatus may be mentioned:

(a) The electron beam can now be centered on the target, by observing the visual luminescence produced by the electron beam in a thin CsBr(Tl) crystal, which can be brought into the target position. A bright beam spot can be seen from the control room through a telescope and two mirrors. This fluorescing crystal method (due to Mr. A. W. Knudsen) became possible when the aluminum window of the scattering chamber was replaced by a 6-mil "Mylar" window, the transparency of which permits observation of the inside of the scattering chamber. During a 12-hour run no drifts in the beam-spot position larger than 1/16 in. occur.

(b) A secondary emission beam monitor of the type described by Tautfest and Fechter[12] has been installed inside the scattering chamber just beyond the scattering target. The secondary emission monitor has been found to have a linear response up to full electron-beam intensity and now replaces the helium ion-chamber monitor, which in previous use was found to be slightly nonlinear.

The Čerenkov counter which we use for detecting the scattered electrons is carefully shielded with lead and paraffin. On the average only one background pulse in two minutes has been registered under conditions of full electron beam, target in place, closed analyzing magnet slits, and magnet at 90°. With open slits, typical counting rates of 50 to 100 counts in the same time period are obtained.

In most of the experiments described here an energy spread of 0.5 percent of the energy in the primary electron beam was chosen. The beam spot at the target was approximately $\frac{3}{8}$ in. wide and $\frac{1}{8}$ in. high. In all experiments the target was held at an angle of 45° with respect to the direction of the primary beam.

The collision energy loss of the electrons in the target was a maximum in the case of Ca, where it was approximately one Mev. The loss of energy due to recoil of the target nucleus, at 183 Mev and at a scattering angle of 90°, amounts in Ca to 0.9 Mev, and in Au to 0.18 Mev.

The angular resolution of the scattering experiment depends mainly on the multiple scattering of the primary electrons in the target, on the finite acceptance angle of the analyzing magnet, and on the finite size of the beam spot. Multiple scattering is the main effect limiting the target thickness. The multiple scattering angle was kept smaller than ±1.5°. For Au a maximum target thickness of 5 mils at 183 Mev (target angle 45°) was used. The acceptance angle (in the scattering plane) of the analyzing magnet was adjusted to ±1.5°. In the preparation of the theoretical scattering curves the finite experimental angular resolution has been taken into account (see Sec. III).

A major problem in these experiments was to separate elastic scattering events from inelastic scattering events. By an inelastic scattering event we understand here an event in which the bombarding electron gives up some of its energy to the target nucleus, which is thereby left in an excited state. Inelastic scattering in high-energy scattering experiments has been observed in Be,[13] C,[14] Mg,[15] Si,[15] S,[15] and Sr,[15] and in other nuclei.

In all of our experiments the number of counts per unit integrated beam is measured for various magnet current settings. Thus an elastic peak is obtained and in some cases one or more inelastic peaks, depending on the target nucleus and on the scattering angle, are found. In Fig. 1 a typical elastic peak is shown for Ca together with a small inelastic peak superimposed on the bremsstrahlung tail of the elastic peak. The number of counts is plotted *vs* energy of the scattered electron. In this particular case the inelastic peak is small and well separated from the elastic peak.

The best energy resolution of the scattering apparatus obtained in these studies corresponds to a peak width energywise of 0.4 percent (full width at half-maximum). It is therefore possible to recognize inelastic contributions arising from excitation of nuclear levels with energy down to approximately 300 kev. For the nuclei

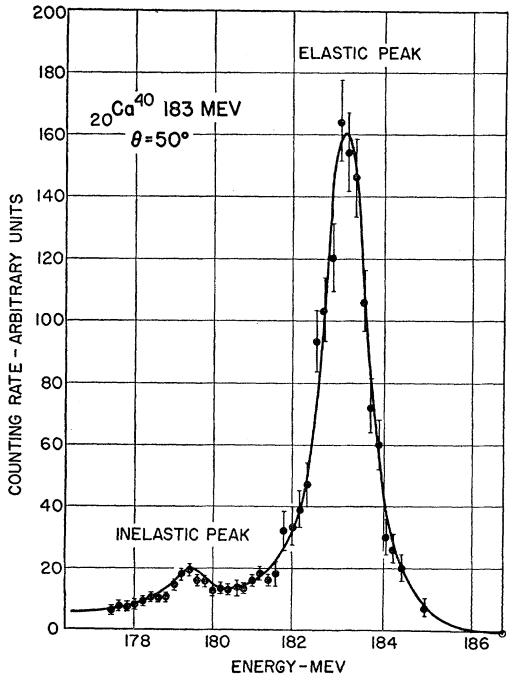

FIG. 1. A typical curve of counting rate *vs* electron energy for calcium at 183 Mev and $\theta = 50°$.

[12] G. W. Tautfest and H. R. Fechter, Phys. Rev. **96**, 35 (1954); Rev. Sci. Instr. **26**, 229 (1955).

[13] McIntyre, Hahn, and Hofstadter, Phys. Rev. **94**, 1084 (1954).
[14] J. Fregeau and R. Hofstadter, Phys. Rev. **99**, 1503 (1955).
[15] R. H. Helm and R. Hofstadter (to be published).

Ca, V, Co, In, Sb, Au, and Bi inelastic scattering was either clearly resolved from the elastic events or else no evidence from line shape studies for an appreciable inelastic scattering contribution down to 300 kev was found.

As a measure of the differential elastic cross section, a sum of the counting rates at 6 points defining an elastic peak was usually taken. No absolute cross sections have been measured so far. Results with any given target material are however subjected to a kind of standardization by associating the measurement at each angle with a corresponding measurement using a standard Au target. After correcting for the target thicknesses, cross section ratios with respect to Au become available. In Sec. IV these ratios will be compared to the theoretical ratios (see Table II). The individual Au runs agree with one another at each angle almost to within the counting statistics. At angles smaller than 90° the statistical error amounts to ±5–7 percent.

The over-all accuracy of the relative cross sections obtained in these experiments is of the order of ±10 percent. At least half of this error is due to counting statistics. The remainder has to be ascribed to drifts in various parts of the experimental equipment. No corrections were found to be important enough to be applied to the direct experimental data and no background effects need to be subtracted. A discussion of possible sources of corrections has been given in earlier papers.[1,2,6]

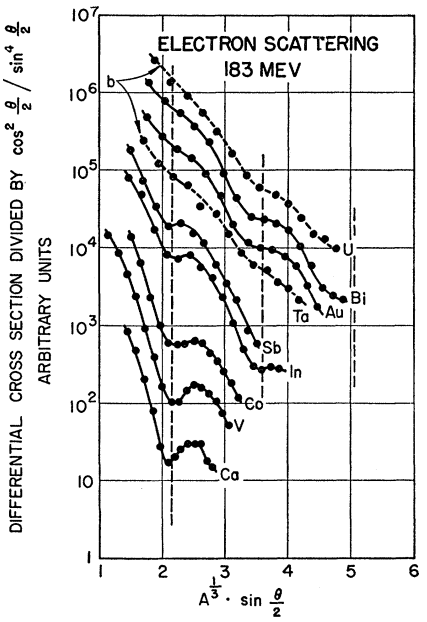

FIG. 2. Experimental results for several nuclei. The differential cross sections, divided by $\cos^2(\theta/2)/\sin^4(\theta/2)$ to display diffraction structure, are plotted *vs* $A^{\frac{1}{3}}\sin(\theta/2)$. The solid lines are smooth curves drawn through the experimental points. They have been shifted arbitrarily in the y-direction. The dashed vertical lines indicate approximately the location of the first, second and third diffraction dips.

III. THEORY

A. Introduction

The experimental results for Ca, V, Co, In, Sb, Ta, Au, Bi, and U are represented in Fig. 2. In order to display diffraction structure, the experimental cross sections have been divided by the angular factor $\cos^2(\theta/2)/\sin^4(\theta/2)$. (This factor is proportional to the theoretical cross section for point scattering obtained using the first Born approximation.) From Fig. 2 and Fig. 13, we see that while for the nuclei Ca, V, Co, In, Sb, Au, and Bi the cross sections show pronounced diffraction structure, this structure is much less marked for the nuclei Hf, Ta, W, Th, and U. The experiments thus separate the nuclei we have examined into these two groups, which we shall call (a) and (b), respectively. In this paper we shall analyze the results of only group (a) nuclei.

The nuclei of group (a) are believed to have little or no "intrinsic deformation" in the Bohr-Mottelson sense,[16] and the electron scattering is elastic. The nucleus can therefore be represented by a static, spherically symmetric charge distribution. The electrostatic potential due to an assumed nuclear charge distribution is obtained numerically. The differential cross section for electron scattering is then calculated by means of a partial wave analysis of the Dirac equation for an electron moving in this potential.[17] This analysis, which is also performed numerically,[18] is very complicated; for gold at 183 Mev, for example, the first ten phase shifts are modified appreciably by the finite nuclear size. The relation between charge distributions and differential cross sections is therefore known to us only empirically, as it were, from experience with many such calculations. One relationship, namely that between the observed diffraction structure and the relatively abrupt nuclear surface, shows up very clearly. This might also be inferred from the first Born approximation, which predicts smooth cross sections for smooth charge distributions such as the Gaussian shape $\rho=\rho_0\exp(-r^2/a^2)$, but undulating cross sections with diffraction zeros for the uniform and "smoothed uniform" shapes.[19,20] As can be seen from Fig. 2, the experimentally observed diffraction structure becomes more pronounced for the lighter elements, where the Born approximation is more reliable. This approximation also predicts that the diffraction structure is a function of $[2E_0R\sin(\theta/2)]/\hbar c$, where E_0 is the electron

[16] A. Bohr and B. R. Mottelson, Kgl. Danske Videnskab. Selskab, Mat.-fys. Medd **27**, No. 16 (1953).

[17] A detailed description of this calculation was given in reference (3).

[18] These calculations were performed on the computer Univac at the University of California Radiation Laboratory at Livermore (unpublished).

[19] J. H. Smith, Ph.D. thesis, Cornell University, 1951 (unpublished); Phys. Rev. **95**, 271 (1954).

[20] L. I. Schiff, Phys. Rev. **92**, 988 (1953).

energy, and R the nuclear radius. Hence the fact that diffraction dips of the same order occur at approximately the same value of $A^{\frac{1}{3}}\sin(\theta/2)$, which is displayed in Fig. 2 by using $A^{\frac{1}{3}}\sin(\theta/2)$ as the scale for the abscissa, indicates that some parameter describing the radius varies roughly as $A^{\frac{1}{3}}$ from element to element. This prediction is confirmed by the detailed analysis presented in the next section.

The nuclei of group (b) all have properties indicative of collective motion of their outer nucleons.[16] (Evidence for this from other experiments is cited at the end of Sec. IV.) Hence we expect contributions to the electron scattering arising from the asymmetry of their charge distributions, and from transitions to their "rotational" levels, which are so low in energy as to be unresolvable in these experiments. It can be shown that for suitably chosen nuclear parameters these contributions fill in the diffraction dips to yield smooth cross sections, like those observed experimentally. The analysis of this process will be given in another report.[21] Some of the nuclei of group (a) show properties characteristic of a little collective nuclear motion, also, but to a negligible extent as regards the electron scattering.

B. Charge Distributions

As is to be expected, for a given experimental error the amount of detail that can be observed in the charge distribution is limited by the electron's reduced de Broglie wavelength, which at 183 Mev is 1.08×10^{-13} cm. Let us first consider "smoothed uniform" charge distributions, for which the charge density is roughly uniform in the central regions, with a smoothed-out surface. We have used the following functional forms:

Fermi:

$$\rho(r)=\rho_1/\{\exp[(r-c)/z_1]+1\}; \tag{1}$$

Modified Gaussian[22]:

$$\rho(r)=\rho_2/\{\exp[(r^2-c^2)/z_2{}^2]+1\}; \tag{2}$$

Trapezoidal:

$$\begin{aligned}\rho(r)&=\rho_3, \quad 0<r<c-z_3,\\ &=\rho_3(c+z_3-r)/2z_3, \quad c-z_3<r<c+z_3,\\ &=0, \quad r>c+z_3.\end{aligned} \tag{3}$$

Experience has shown us that at energies up to 183-Mev differential cross sections depend essentially on only two parameters, a mean radius and a surface thickness, and are almost independent of the particular analytic form used for ρ. Roughly speaking, the radius determines the angular position of the diffraction dips, and the surface thickness their depth. Of course, for each of the above shapes the parameter c adjusts the radius, while the surface thickness is related to z_1, z_2, and z_3 in (1), (2), and (3), respectively. But the exact relationship among the parameters of equivalent shapes [i.e., particular examples of (1), (2), and (3) which yield almost identical differential cross sections] is known to us only numerically. Approximate relationships can be obtained by using the fact that the electron wave functions in the neighborhood of the nucleus are approximately plane waves with modified amplitude and argument.[21] A simple analysis on the lines of the Born approximation then shows that the scattering depends, to lowest order in $(s/c')^2$, on the quantities c' and s defined by the relations

$$c'=\int_0^\infty \rho(r)dr/\rho(0), \tag{4}$$

$$s^2=-4\int_0^\infty (r-c')^2\rho'(r)dr/\rho(0). \tag{5}$$

c' is the distance at which ρ has dropped to half of its value at the center, and s is proportional to the rms thickness of the surface. (The last two statements are true strictly for only (1) and (3), where ρ obeys the additional condition that $\rho(c'+\delta)=\rho(0)-\rho(c'-\delta)$.) Since the value of s is found to vary appreciably with the functional form of ρ, we quote in our results also t, the distance over which ρ drops from 0.9 to 0.1 of its central value. It turns out that t is less dependent on the form of ρ than s. Since the rms radius has been used extensively in the literature as a measure of nuclear radius, we quote also R, which is proportional to it:

$$R=(5\langle r^2\rangle/3)^{\frac{1}{2}}. \tag{6}$$

We shall also use $r_0=A^{-\frac{1}{3}}R$ and $r_1=A^{-\frac{1}{3}}c$. The quantities c, s, and R are connected by the approximate relation

$$R^2\simeq c^2[1+(5s^2/2c^2)]/[1+(3s^2/4c^2)].$$

The surface parameters s and t are related to the quantities occurring in (1), (2), and (3) as follows: (1), the Fermi shape, $s=2\pi z_1/\sqrt{3}=3.63z_1$, $t=(4\log_e 3)z_1=4.40z_1$; (2), the modified Gaussian shape, $t=(c^2+2z_2{}^2\log_e 3)^{\frac{1}{2}}-(c^2-2z_2{}^2\log_e 3)^{\frac{1}{2}}\simeq 2.20z_2{}^2/c$ (the expression for s is only known to us numerically for special cases); (3), the trapezoidal shape, $s=2z_3/\sqrt{3}=1.15z_3$, $t=1.60z_3$. In terms of these quantities the central charge density is given by

$$\rho(0)=3Ze/\{4\pi c^3[1+(3s^2/4c^2)]\}. \tag{7}$$

The effect of a variation in the central charge density has been examined in gold by using the functional form

$$\rho(r)=\rho_8[1+(wr^2/c^2)]/\{\exp[(r-c)/z_8]+1\}. \tag{8}$$

Since this variation turns out to have little influence on the cross sections, we have used only two-parameter charge distributions in our examination of the other nuclei. Such an effect, if present, will probably show up more clearly when experiments at higher energies include several of the diffraction dips.

[21] Downs, Ravenhall, and Yennie (to be published).

[22] Note that this shape is roughly uniform with a Gaussian surface. It is *not* the Gaussian shape $\rho=\rho_0\exp(-r^2/a^2)$ used previously.

C. Analysis of the Experiments

The present procedure for finding the nuclear charge distributions predicted by the experimental cross sections is necessarily one of successive trials. For any assumed charge distribution the cross section obtained by means of the phase-shift analysis is folded over a small angular range to allow for the finite experimental resolution. We assumed a Gaussian distribution,

$$\bar{\sigma}(\theta)=(\pi^{\frac{1}{2}}\Delta)^{-1}\int_{-\infty}^{\infty}\sigma(\theta')\exp[(\theta-\theta')^2/\Delta^2]d\theta', \quad (9)$$

and for Δ have used the fixed value of 2°. This is intended to represent approximately a spread in incident beam energy, multiple scattering in the target and finite beam size, besides the acceptance angles of the spectrometer (usually $\pm 1.5°$).

Comparison with experiment is made by least squares. The probability that theory and experiment are in agreement is

$$P=\prod_i \exp\{-[(\sigma_i/\lambda\epsilon_i)-1]^2N_i/2\}, \quad (10)$$

where σ_i is the theoretical cross section at θ_i, and ϵ_i and N_i are, respectively, the experimental value and the number of counts. The parameter λ is required because the experimental cross section is not known absolutely, and we therefore maximize P with respect to λ. The maximum occurs when $\lambda=M_2/M_1$, where $M_n=\sum_i(\sigma_i/\epsilon_i)^nN_i$; for this value of λ the logarithm of the probability is given by

$$-\log P=\tfrac{1}{2}(M_0M_2-M_1^2)/M_2. \quad (11)$$

Thus, for each theoretical cross section we calculate (11) and then look for the values of r_0 and s which make it a minimum. This is then the best fit for that particular shape. We can thus compare the relative merits of various shapes, and also have an idea of the error in our results due to statistics. A comparison of results for various experimental runs in gold shows us the error due to any slight lack of repeatability in the experiments. We discuss this more fully in the next section.

D. Other Effects

For simplicity we ignore radiative corrections to scattering in the above analysis. Suura[23] has shown that, independently of Z, the relative correction to the cross section is to a good approximation the same as was calculated by Schwinger[24] using the Born approximation. For typical experimental conditions ($E=183$ Mev, $\Delta E/E=0.5$ percent) Schwinger's analysis predicts a relative change in the theoretical cross sections between 35° and 120° of 4.3 percent. Since the radiative correction varies smoothly with angle, however, its inclusion would make the theoretical cross section a little steeper while not altering its detailed shape. This would decrease the surface thickness of the predicted charge distribution a little (~0.4 percent), and would not alter the radius appreciably. In view of possible uncertainties in the theoretical analysis, and of their small and easily predicted effect, it seemed better to omit radiative corrections altogether.

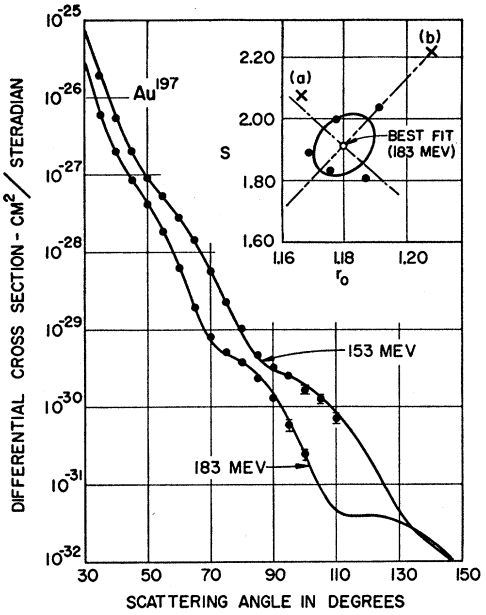

FIG. 3. Angular distributions for gold. The experimental points at 183 Mev are the average of five runs. The solid curve at 183 Mev is the theoretical best fit obtained by using the Fermi smoothed uniform charge distribution (1). It corresponds to the open circle in the inset figure of s *vs* r_0. Its coordinates are the weighted average of those corresponding to the best fits for the individual runs, represented by the points. The ellipse in the inset figure corresponds to charge distributions for which the probability of agreement with experiment is half of its maximum value, attained for the best fit. The crosses (a) and (b) correspond to charge distributions whose parameters differ from those of the best fit by about two probable errors. Their cross sections are shown in Fig. 4. The solid curve at 153 Mev is for the same parameters as the best fit at 183 Mev. Numerical values of the parameters for all of the nuclei are given in Table III.

For those nuclei of group (a) having nonzero spin values and magnetic moments, there should be a magnetic dipole contribution to the elastic scattering. Since the magnetic moment (μ) arises in the surface region of the nucleus, this contribution can be expected to show about the same dependence on the finite nuclear size as the charge scattering. The ratio of these two contributions will thus vary approximately as $(\mu/Z)^2$, so that although the magnetic effect is appreciable for hydrogen,[25,26] it is negligible at this energy for the nuclei examined here.

The analysis of the elastic scattering in terms of static charge distributions is quite general, but the

[23] H. Suura, Phys. Rev. **99**, 1020 (1955).
[24] J. Schwinger, Phys. Rev. **76**, 780 (1949).
[25] R. Hofstadter and R. W. McAllister, Phys. Rev. **98**, 217 (1955).
[26] M. N. Rosenbluth, Phys. Rev. **79**, 615 (1950).

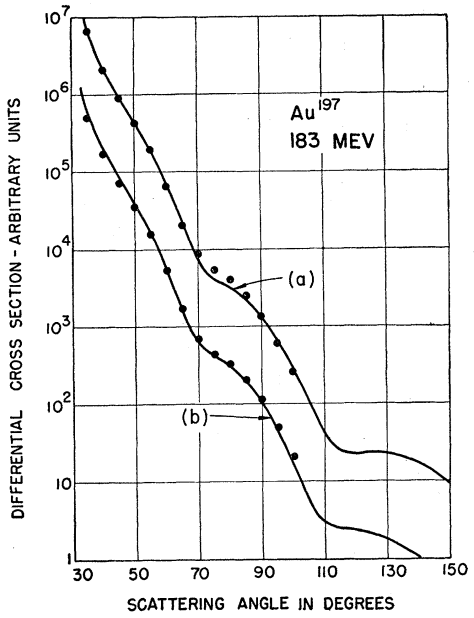

FIG. 4. Comparison with experiment at 183 Mev of cross sections for charge distributions whose parameters differ by about two probable errors from those of the best fit. They correspond to the crosses (a) and (b) in the inset in Fig. 3. In vertical scale one of the cross sections has been shifted by a factor 10 for clarity.

connection between this charge distribution and the nuclear wave function may not be so direct. Although the major part of $\rho(r)$ comes from $|\Psi_{\text{ground}}(r)|^2$, there will also occur, in higher orders of the perturbing interaction between the electron and the nucleus, contributions involving nuclear excited states arising from virtual excitation. For light nuclei Schiff,[27] using the Born approximation, has estimated that this "dispersion scattering" is only about 1/137 of the scattering from the ground state alone. In our analysis this effect would show up as a contribution to the charge distribution which might be energy-dependent, because of the energy denominators in the perturbation theory. In Sec. IV we have analyzed the scattering from Bi at both 153 and 183 Mev, but the results at the two energies are probably not significantly different.

Our calculations assume the Coulomb law of force between the electron and each element of the nuclear charge. Any alteration in the law of force at small distances would modify the relationship between the charge distributions and the potentials used in the Dirac equation. Correction of our results to allow for this effect would not involve much recalculation. From the *potentials* corresponding to our quoted best fits the altered relationship between potential and force law would immediately give us the modified charge distributions. There is at present no strong evidence for such an altered force law.

[27] L. I. Schiff, Phys. Rev. 98, 756 (1955).

IV. RESULTS

Gold.—In gold-197 there are five experimental runs at 183 Mev. The average of these runs is shown in Fig. 3 together with the theoretical best fit using shape (1), which has been folded to allow for finite experimental resolution. Inset in that figure are points indicating the values of r_0 and s for the best fits to the individual runs at 183 Mev. Corresponding to each of these points, for which P, the probability of agreement between theory and experiment, is a maximum, there is a curve describing charge distributions for which P is a half of its maximum value. Since we are close to the best fit, this curve is of only second degree in r_0 and s, i.e., it is an ellipse. It tells us the error due to statistics. The scatter of these points about their mean (measured by using as weighting factor $\sum N_i$, the total number of counts in the run) arises both from statistics and from a slight lack of repeatability of the runs. Our analysis indicates that the latter is only about half as important as the former. The ellipse shown in the inset figure combines both sources of error. In Fig. 4 we compare with experiment the cross sections of two shapes whose parameters differ from those of the best fit by about two probable errors. (They correspond to the crosses in the inset to Fig. 3.) We feel that these are a significantly poorer fit to experiment than the shape chosen in Fig. 3; this shows that the estimates of error given by the least squares analysis are in rough agreement with intuitive ideas obtained from inspection.

A feature of our results which is not too marked for gold, but which is very noticeable for the lighter elements, is that the major axis of the ellipse corresponds to shapes with the same value of the radial parameter c. This means that c is the parameter that can be specified most accurately, a result which agrees with our experience that the angular position of the diffraction dips, the most prominent feature of the cross section, is determined mainly by c. The eccentricity of the ellipses increases for the lighter elements, implying that for these elements the accuracy of s decreases relative to the accuracy of c. This is linked with the fact that in the diffraction dips, the angular region where the surface thickness is most evident, the agreement between theoretical and experimental cross sections is poorer for the light elements than for the heavy elements. The

TABLE I. Results of the analysis of the gold experiments at 183 Mev. The first three shapes are two-parameter shapes of the smoothed uniform type, while the fourth contains an additional parameter which allows alteration of ρ in the central region. All lengths are in units of 10^{-13} cm, and the charge density in units of 10^{19} coulomb/cm^3. The accuracy of the radial parameters c, c', and R is about ± 1 percent; for the surface thickness parameter t it is about ± 5 percent.

Shape	c	z_i	w	c'	R	s	t	ρ_0
(1) Fermi	6.38	0.535	···	6.38	6.88	1.94	2.35	1.09
(2) Modified Gaussian	6.36	2.72	···	6.17	6.85	2.04	2.61	1.13
(3) Trapezoidal	6.28	1.49	···	6.28	6.66	1.72	2.39	1.15
(8) 3-parameter	6.07	0.613	0.64	···	6.92	···	···	0.85

errors in the results on the other elements are in any case somewhat larger than those for gold, since the results are less numerous (usually only two runs for each element). For all of the above reasons, the errors quoted at the beginning of Sec. V should be regarded as orders of magnitude rather than precisely known quantities.

To examine the experiments on gold for dependence on surface shape, the same procedure as that just described for shape (1) was followed for shapes (2) and (3). The maximum values of P for the three cases were found all to lie within a factor 1.3 of each other, i.e., the agreement with experiment is not significantly different for the three shapes. The values of the parameters for the best fits are presented in Table I. The variation in the radial parameters quoted is very small: in c [the parameter occurring in the definitions (1), (2), and (3)] it is 1.6 percent, while in c' [defined by the integral relation (4)] and in R [proportional to the rms radius, as defined by (6)] it is 3.3 percent. There is a much larger variation in the parameters describing the surface thickness, as is to be expected, although t, the distance over which ρ drops from 0.9 to 0.1 of its central value, varies less (10 percent) than s, defined by the integral relation (5) (17 percent). It should be possible to define a radial and a surface parameter so that their values are independent of shape, but as these results show, we have been able to do this only in an approximate way. The charge distributions corresponding to the best fits for shapes (1), (2), and (3) are shown in Fig. 5. It is remarkable how closely they agree over the surface region, especially at the two outermost points of intersection. Needless to say, the cross sections corresponding to these charge distributions differ so little that Fig. 3 can be taken to represent also shapes (2) and (3), with a slight shift in the vertical scale.

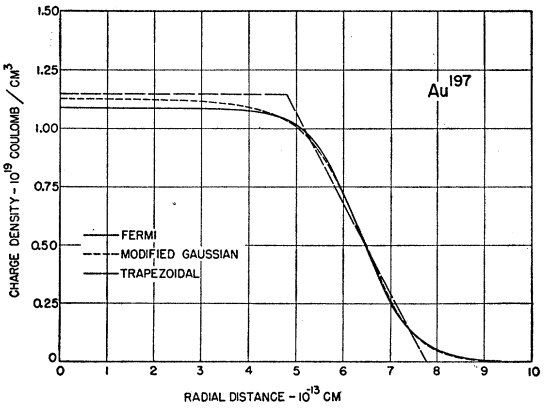

FIG. 5. Three charge distributions in gold, the best fits to the experimental results at 183 Mev for the Fermi, modified Gaussian, and trapezoidal shapes (1), (2), and (3); the charge distribution parameters are listed in Table I. The cross section for the Fermi best fit is shown in Fig. 3; those for the other two shapes differ from it only slightly.

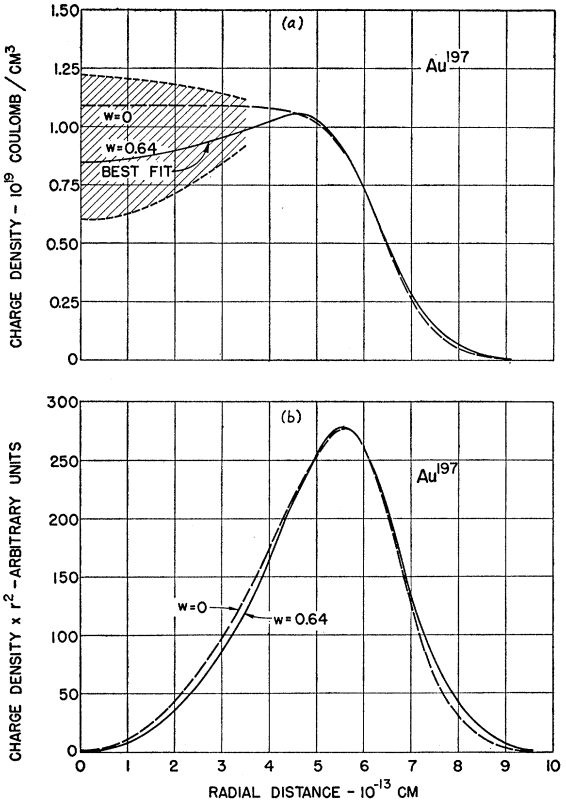

FIG. 6. (a) Charge distributions in gold obtained using shape (8), which allows variations in the charge density near the center. The full curve is the best fit to the experimental data at 183 Mev, and the two dotted curves give cross sections for which the probability of agreement between theory and experiment (10) is a half of its value for the best fit. The dashed curve, drawn for comparison, is the best fit using shape (1). (b) The charge distributions represented by the full and dashed curves in (a) have been multiplied by r^2, to show the distribution of the actual amount of charge with radius.

We have used shape (8) to detect any dependence of the cross section on the central charge density. The procedure is closely similar to the preceding ones: for chosen values of w, the parameter fixing the variation in central charge density, the best fit for varying z_8 and c is obtained. We then minimize (11) with respect to w. The "best" value of w corresponds to a ratio $\rho(0)/\rho_{\max}$ of 0.80; the value of P is 1.5 times its value for the Fermi smoothed uniform shape (1), a difference which lies within the probable error. The charge distribution is shown in Fig. 6, and the cross section is almost indistinguishable from that shown in Fig. 3. It turns out that the cross sections are rather insensitive to w so that the limits that can be put on w are rather wide. The reason for this weak dependence on w is clear from Fig. 6, in the plot of $r^2\rho(r)$, the amount of charge at a distance r from the center, *vs* r. We see that what looks from the plot $\rho(r)$ *vs* r to be an important alteration in shape actually involves the shifting of only a small amount of charge. This is, of course, why our analysis predicts most accurately the

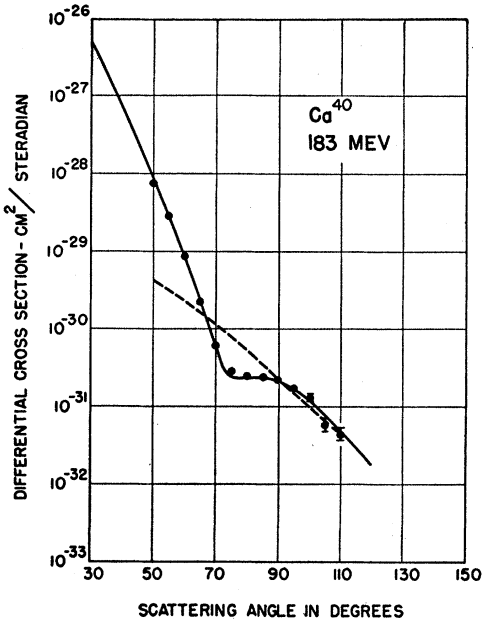

FIG. 7. Experimental and theoretical cross sections for the scattering of 183-Mev electrons by calcium. The full line in this figure, and in Figs. 8–12, is the theoretical best fit at 183 Mev obtained by using shape (1). The dashed line in this figure is the experimental cross section for the inelastic scattering corresponding to excitation of nuclear levels at about 3.7 Mev.

position of the nuclear surface—that is, the place where most of the charge resides.

To summarize, the analysis of gold-197 yields the results that first, there is no discernible dependence on the details of the shape of the surface of the charge distribution, although the relation between parameters of equivalent charge distributions is known only numerically; secondly, there is only a weak dependence on the variation in the central density, and the best fit has charge density almost uniform in the center. Hence, in our analysis of the other elements, which we do in order of increasing Z, we have used only shape (1). With the assumption that the relations between parameters of equivalent shapes is the same for the other elements as those found in gold (Table I), the numerical results, presented in Table III, can be reinterpreted in terms of shapes (2) and (3), respectively, by scaling the parameters therein as follows: c, by factors 1.00 and 0.98; R, by factors 0.99 and 0.97; and t, by factors 1.11 and 1.02.

The experimental angular distributions for the nuclei Ca, V, Co, In, Sb, and Bi together with their best theoretical fits (using Fermi smoothed uniform charge distributions) are shown in Figs. 7–12. The errors quoted in these figures are only due only to counting statistics. For small angles, where no error is indicated, this error is smaller than 10 percent. All nuclei in this group, except Sb, have an isotopic purity greater than 95 percent. The target thicknesses, measured in mils, were 120 (Ca), 26 (V), 42 (Co), 10 (In), 15 (Sb), and 10 (Bi). The results for the individual nuclei will now be discussed briefly.

Ca.—(Fig. 7.) A natural Ca target containing 96.9 percent of doubly magic Ca^{40} was used. Besides the elastic scattering peak a strong inelastic peak has also been found, which is probably due to excitation of the known levels in Ca at 3.73 and 3.90 Mev. There seems to be no evidence for the lowest known level in Ca at 3.35 Mev (0^+) from this experiment. The angular distribution of the inelastic scattering is indicated by the dashed line in Fig. 7. As can be seen from Fig. 1, the inelastic scattering in Ca was easily separated from elastic scattering. Between 70° and 80° there appears, approximately 1 Mev down from the elastic peak, an additional small inelastic peak, the origin of which is unknown to us.

V.—(Fig. 8.) 99.75 percent of natural V is V^{51}. This nucleus has a level at 320 kev, which, if excited in our experiment, should show up as a broadening of the elastic peak. No evidence for such an effect was seen, and there is probably no more than 10 percent inelastic contribution to the measured cross section at any angle. Such an inelastic contribution would not alter the values of the charge distribution parameters by more than the quoted errors.

Co.—(Fig. 9.) Co^{59} (natural Co) is known to have excited states at approximately 1.1 and 1.3 Mev. Some evidence has been found in this experiment for excitation of several levels above 1 Mev, the relative cross section with respect to the elastic cross section being largest at about 65° and amounting to approximately 20 percent. This elastic scattering has been resolved experimentally.

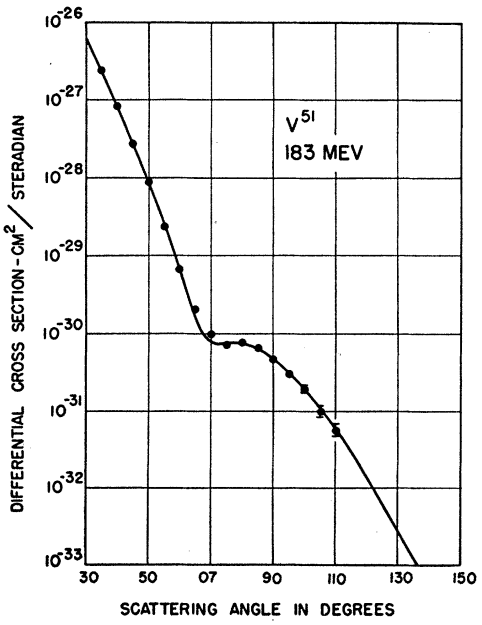

FIG. 8. Experimental and theoretical cross sections for the scattering of 183-Mev electrons by vanadium. (In the abscissa, 07 should be 70.)

In.—(Fig. 10.) Natural In contains 95.8 percent In^{115} and 4.2 percent In^{113}. In a high-resolution run, 0.8 Mev full width at half-maximum of the elastic peak, no inelastic peaks have been found. The charge distribution parameters obtained from a least square fit to the 813-Mev data have been used to calculate the theoretical angular distribution at 153 Mev, yielding a curve which is in good agreement with the experimental data.

Sb.—(Fig. 11.) Natural Sb contains approximately half and half Sb^{121} and Sb^{123}. Sb^{123} has a known level at 0.15 Mev. This level, if excited in our experiment, could not be resolved from elastic scattering. The measured cross section therefore may include some inelastic contribution. We know however from our inelastic scattering work that the relative inelastic scattering contribution becomes in general smaller by going to large nuclei, with the possible exception of nuclei with large distortions from spherical symmetry (like Hf, Ta, W, etc.).

Au.—(Fig. 3.) The low-lying levels in Au at 77 and 268 kev, which have been excited in Coulomb excitation experiments, are believed to give no appreciable contribution to the measured cross sections. According to calculations by Downs *et al.*,[21] such a contribution becomes important only at very large scattering angles, amounting to about 10 percent at the third diffraction dip at 115°. A line-shape study of the Au peaks did not reveal any broadening of the peaks by going to large angles. The theoretical Au curve at 153 Mev is obtained by using the same charge distribution parameters as gave the best fit at 183 Mev.

Bi.—(Fig. 12.) The lowest known levels in Bi^{209} (natural Bi) lie at 0.91 and 1.63 Mev. No experimental evidence has been found for the excitation of these levels by 183-Mev electrons. The angular distributions at 183 and 153 Mev have each been analyzed theoretically and the best fits are plotted in Fig. 12. The values of the parameters are $r_0=1.201$, $s=2.25$, and $r_0=1.214$, $s=2.03$, respectively. These values agree to within the errors quoted in Sec. V.

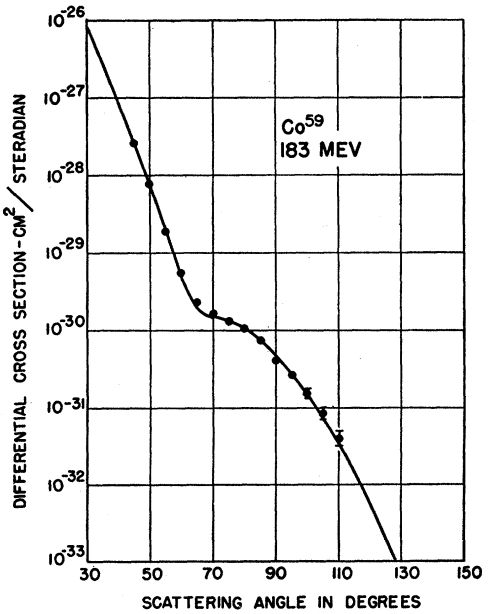

FIG. 9. Experimental and theoretical cross sections for the scattering of 183-Mev electrons by cobalt.

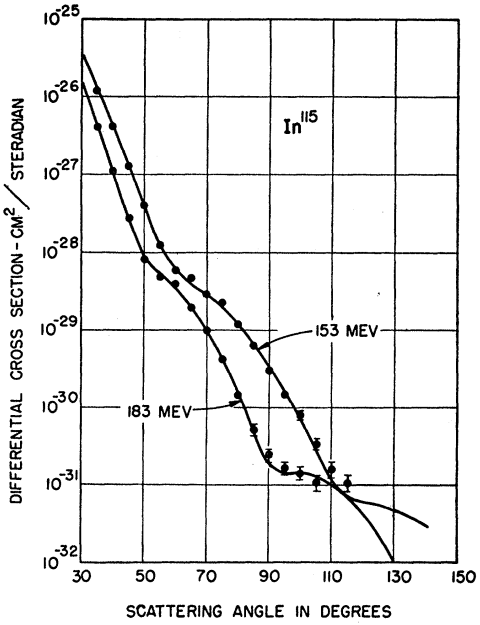

FIG. 10. Experimental and theoretical cross sections for the scattering of 183- and 153-Mev electrons by indium. The theoretical cross section at 153 Mev is calculated for the same parameters as the 183-Mev result.

A valuable check on the consistency of the theoretical results has been obtained by comparing the experimental cross section ratios (with respect to Au) with the corresponding theoretical ratios. An average cross-section ratio over the five smallest angles measured has been chosen. The experimental ratios divided by the theoretical ratios are listed in Table II. In view of the fact that cross sections vary by large factors with changes in angle and from element to element, these ratios are remarkably close to unity.

In Fig. 13 angular distributions at 183 Mev for the nuclei Hf, Ta, W, Th, and U are plotted. The fact that these curves show almost no diffraction structure is believed to be connected with distortion of nuclear matter from spherical symmetry. All of these nuclei have low-lying nuclear levels which are strongly excited by Coulomb excitation, indicating high intrinsic quadrupole moments. The averages for natural Hf, Ta, and W of the intrinsic quadrupole moments deduced from measurements of the γ-ray yield in Coulomb excitation are approximately 10, 4, and 7 barns, respectively.[28] The quadrupole moments of Th and U are

[28] McClelland, Mark, and Goodman, Phys. Rev. **97**, 1191 (1955).

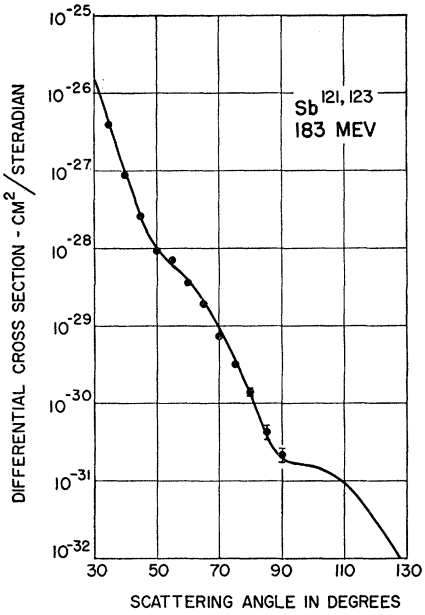

FIG. 11. Experimental and theoretical cross sections for the scattering of 183-Mev electrons by antimony.

not known to us. There are, however, levels at 50 and 44 kev for U, found by Coulomb excitation, suggesting large nuclear distortion. An analysis of electron scattering from such nuclei will, as mentioned in Sec. III, be presented in another report.[21]

V. DISCUSSION

Results of the analysis of gold, the nucleus studied most intensively in this investigation, are presented in Table I and Fig. 3, and have been commented on fully in Sec. IV. Briefly, the following information has been obtained about the charge distribution: while not too much can be said about the central region, except that ρ is probably fairly flat, the surface region is now known with the following precision: the radius c (the distance to the half-point) is 6.4×10^{-13} cm, accurate to about $\pm$ one percent, and the surface thickness t (the 0.9 to 0.1 distance) is 2.4×10^{-13} cm, accurate to about ±5 percent, although the precise values depend slightly on the particular shape chosen. These values are in agreement with the preliminary prediction of Ravenhall and Yennie,[4] and with analyses of our earlier data by Brown and Elton[7] and by Hill *et al.*[8]

The charge distributions for all of the nuclei examined are plotted in Fig. 14, and the values of the various parameters are given in Table III. The choice of the Fermi smoothed uniform shape has no special significance, and the formulae for converting the results to apply to the other two-parameter shapes, assumed to be the same as for gold, are given in Sec. IV. As regards the accuracy of the entries in Table III, we feel that as an order of magnitude the errors can be said to be about twice those quoted for gold, i.e., ±2 percent for radial parameters, and ±10 percent for the surface thicknesses. These errors are, however, difficult to estimate and, as mentioned in Sec. IV, the error in s for the lighter elements may be a little larger. Not included is a possible error due to uncertainty in the energy of the primary electron beam, estimated to be smaller than 1 percent. This uncertainty would affect all data by the same amount, and in the same direction.

To examine the dependence of the radial parameters c and R [defined by (4) and (6)] on A and Z, the quantities $r_0=R/A^{\frac{1}{3}}$, $r_1=c/A^{\frac{1}{3}}$, and $r_2=R/(2Z)^{\frac{1}{3}}$ are also given in Table III. r_0 varies appreciably with A, but both r_1 and r_2 are remarkably constant from element to element, the total variations being only 4 percent and 5 percent, respectively. Our result that r_1 is constant means that for the nuclei we have investigated the midpoint of the surface of the charge distribution varies as $A^{\frac{1}{3}}$ to within ±2 percent. These results are to be compared with those of Fitch and Rainwater,[9] who measured level splitting in the mu-mesonic atoms of Ti, Cu, Sb, and Pb. The analysis of the experiments by these authors and by Cooper and Henley[10] assumes a uniform charge distribution (zero surface thickness), but it appears that at least for the light nuclei the

TABLE II. Experimental cross-section ratios with respect to Au divided by theoretical cross-section ratios with respect to Au for group (a) nuclei. An average cross-section ratio over the five smallest angles measured has been chosen.

Element	Ca	V	Co	In	Sb	Bi
$\frac{(\sigma_X/\sigma_{Au})_{exp}}{(\sigma_X/\sigma_{Au})_{theor}}$	1.06	1.03	0.85	0.95	1.01	1.09

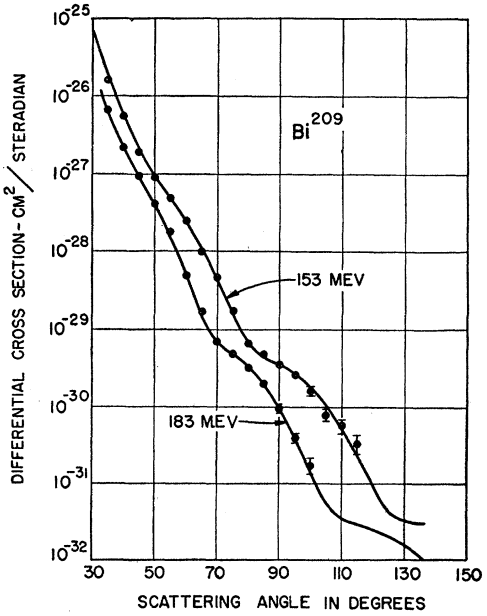

FIG. 12. Experimental and theoretical cross sections for the scattering of 183- and 153-Mev electrons by bismuth. The experiments at the two energies were analyzed separately.

only parameter that can be determined is the rms radius, i.e., R. They find that the radius of the uniform distribution is given roughly by $1.10A^{\frac{1}{3}}\times10^{-13}$ cm for Ti and Cu (assuming a mu-meson mass of 207 electron masses). A more elaborate analysis of their experiments in Pb by Hill and Ford,[11] using charge distributions with finite surface thicknesses, yields the value for r_0 of 1.18×10^{-13} cm, in good agreement with our results. There remains, however, a discrepancy between the values of r_0 obtained from the mu-mesonic atom experiments and from our electron scattering experiments for the lighter nuclei, especially Cu and Ti; we should expect results for these elements to agree with our results on Co, V, and Ca. The origin of this discrepancy is not known to us.§

As regards the other quantities listed in Table III, we note first that the surface thickness t is approximately constant, to within the quoted errors, and equal to about 2.4×10^{-13} cm. Expressed in terms of s [defined by the integral relation (5)], this is 2.0×10^{-13} cm. The central charge density $\rho(0)$, calculated from c and s by means of Eq. (7), is given in units of 10^{19} coulomb per cm^3. For gold, for example, it corresponds to 0.068 proton per $(10^{-13}$ cm$)^3$. It shows a significant decrease

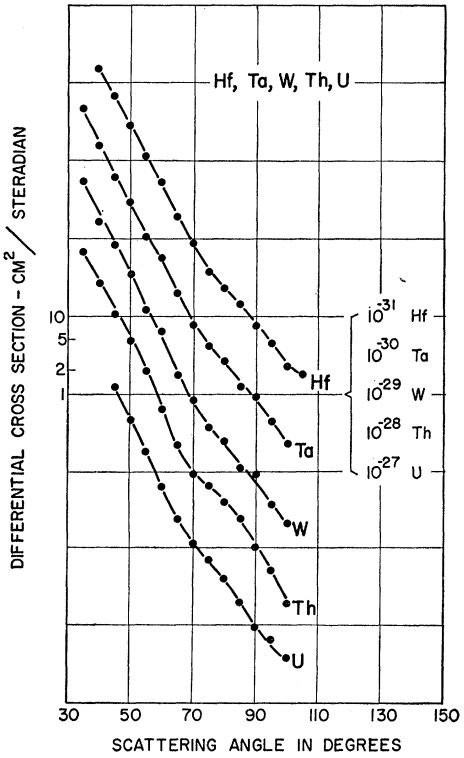

FIG. 13. Experimental cross sections at 183 Mev for the nuclei Hf, Ta, W, Th, and U. Absolute cross sections have been obtained from the counting rate ratio with respect to gold, and from the absolute cross section for gold given in Fig. 3. The dashed lines are smooth curves connecting the experimental points, and are *not theoretical*. The curves have been shifted vertically by factors of ten as indicated.

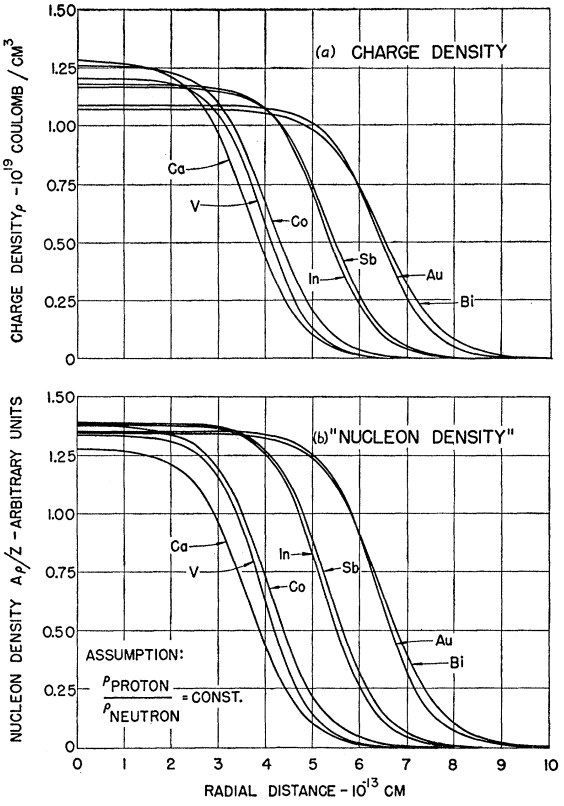

FIG. 14. (a) Charge distributions $\rho(r)$ for Ca, V, Co, In, Sb, Au, and Bi. They are Fermi smoothed uniform shapes, with the parameters given in Table III, and yield the cross sections shown in Figs. 3 and 8–12. (b) A plot of $(A/2Z)\rho(r)$ for the above nuclei. On the assumption that the distribution of matter in the nucleus is the same as the distribution of charge, this represents the "nucleon density."

TABLE III. Results of the analysis of the group (a) nuclei in terms of charge distribution (1), the Fermi smoothed uniform shape. All lengths are in units of 10^{-13} cm, charge densities in 10^{19} coulombs/cm^3, and energies in Mev. The accuracy of these results (except for gold, for which the accuracy is given in the caption of Table I) is estimated as follows: radial parameters, ±2 percent; surface thickness parameter, ±10 percent, although the last figure may be perhaps a little larger for the lighter nuclei. The quantity ρ_0 is the normalization parameter occurring in the definition (1), and physically is probably an average value of ρ for the central regions. It is *not* the actual central density, which cannot be determined accurately from these experiments.

	c	R	$c/A^{\frac{1}{3}}=r_1$	$R/A^{\frac{1}{3}}=r_0$	$R/(2Z)^{\frac{1}{3}}=r_2$	t	ρ_0	E_c
$_{20}Ca^{40}$	3.64	4.54	1.06	1.32	1.33	2.5	1.28	78
$_{23}V^{51}$	3.98	4.63	1.07	1.25	1.29	2.2	1.21	100
$_{27}Co^{59}$	4.09	4.94	1.05	1.27	1.30	2.5	1.26	130
$_{49}In^{115}$	5.24	5.80	1.08	1.19	1.26	2.3	1.18	360
$_{51}Sb^{122}$	5.32	5.97	1.07	1.20	1.28	2.5	1.17	380
$_{79}Au^{197}$	6.38	6.87	1.096	1.180	1.270	2.32	1.09	790
$_{83}Bi^{209}$	6.47	7.13	1.09	1.20	1.30	2.7	1.07	840

§ *Note added in proof.*—Professor E. P. Wigner has kindly pointed out to us that, following his suggestion, B. G. Jancouici (Phys. Rev. **95**, 389 (1954)) made a detailed calculation on the Coulomb energy in the pairs (N^{15}, O^{15}) and (F^{17}, O^{17}) and showed that nuclear radii determined from mirror nuclei data were larger than those obtained by using the results of Fitch and Rainwater for light elements ($r_0=1.2\times10^{-3}$ cm). Thus this discrepancy had been noted earlier.

for the heavy elements. It seems worth noting that if, on the assumption that the distribution of matter in the nucleus is the same as the distribution of charge, we calculate $(A/Z)\rho(r)$, as in Fig. 14(b), the central value of this "nucleon density" remains roughly constant from element to element. In the last column of Table III we give the electrostatic Coulomb energy of the nuclear charge distributions ($E_c=\frac{1}{2}\int\rho(r)V(r)d^3r$). This turns out to be approximately the same as the Coulomb energy of a uniformly charged sphere of radius R.

These results may be summarized as follows: for seven elements between calcium-40 and bismuth-209 the nuclear charge distribution is found to have a radius c (to the midpoint of the surface) of $(1.07\pm.02)A^{\frac{1}{3}}\times10^{-13}$ cm, and a surface thickness t (0.9 to 0.1 distance) of $(2.4\pm0.3)\times10^{-13}$ cm.

ACKNOWLEDGMENTS

The work described in this paper was materially aided by many people, to whom we would like to express our appreciation. On the experimental side we wish to thank Phyllis Hansen, T. O. McKinney, K. H. Sherwin, R. E. Steele, R. M. Friedman, R. H. Helm, R. W. McAllister, and G. W. Tautfest for operation of the accelerator; Dr. H. Mark and Professor C. Goodman for the loan of some hafnium metal; B. R. Chambers and B. G. Stuart for the machining of some of the target foils, and Mr. A. W. Knudsen, Dr. J. A. McIntyre, and Professor J. F. Streib, Jr., for useful discussions. On the theoretical side we would like to thank the authorities of the University of California Radiation Laboratory at Livermore, particularly Dr. S. Fernbach, for the use of the computer Univac, and Dr. G. J. Lasher for assistance in its operation; the staff of the Stanford Computation Center for advice and assistance in the use of the Card-Programmed Calculator; Dr. D. L. Hill for an account of his calculations on electron scattering before their publication; and Dr. D. R. Yennie and Professor L. I. Schiff for helpful discussions. One of us (B.H.) acknowledges with thanks financial help from the Schweizerische Arbeitsgemeinschaft in Mathematik und Physik.

PHYSICAL REVIEW VOLUME 101, NUMBER 3 FEBRUARY 1, 1956

Effects of a Ring Current on Cosmic Radiation

ERNEST C. RAY
Department of Physics, State University of Iowa, Iowa City, Iowa
(Received September 19, 1955)

A theoretical analysis of the effect of an equatorial ring current on the latitude variation of the primary cosmic radiation has been carried out. It has been found that a ring current of the size suggested by Schmidt should lead to observable effects on the latitude variation. In particular, if a ring current of radius equal to 7.5 earth radii and current strength sufficient to produce a field of 100γ at the earth's equator exists, then the knee in the latitude variation is a feature of the rigidity cut-off curve rather than of the primary spectrum. The primary spectrum obtained with the use of geomagnetic theory which includes a ring current is satisfactorily fitted with a function of the form $J=0.29\ E^{-0.9}$ (cm^2 sec sterad)$^{-1}$, where E is the total energy of a primary particle. Certain features of time variations of the cosmic-ray intensity apparently disagree with the theory.

INTRODUCTION AND SUMMARY

IN their theory of magnetic storms and auroras, Chapman and Ferraro[1] speculated that a westward-flowing ring current encircling the earth at the geomagnetic equator with a radius between five and ten earth radii might explain the decrease of the earth's field observed during the main phase of a geomagnetic storm, and perhaps as well serve as a reservoir of particles to produce the auroras during times of no magnetic storm. The present work is an attempt to submit this hypothesis to experiment by exploring the effect of such a ring current on the latitude variation of the primary cosmic radiation. This investigation has been carried out in the Störmer approximation,[2] and hence can be expected to be valid only in directions near the vertical and in a range of latitudes north of about 45° geomagnetic. This range of validity is quite convenient, since it will turn out that the ring current has its greatest effect in those latitudes, and is of comparatively little importance nearer the equator.

The main results found are the following: If the primary spectrum is of the form $J=J_0E^{-\gamma}$, where E is the total energy of the primary particle,[3] then with $J_0=0.29$ and $\gamma=0.9$, a ring current with suitably chosen parameters will produce the observed latitude dependence of the vertical intensity (see Fig. 7). The

[1] S. Chapman and V. C. A. Ferraro, Terrestrial Magnetism and Atm. Elec. **37**, 77 (1931); **36**, 171 (1931); **37**, 147 (1932); **37**, 421 (1932); **38**, 79 (1933); **45**, 245 (1940); **46**, 1 (1941). The ring current is discussed in **38**, 79 and **46**, 1 of the above list of references.

[2] See R. A. Alpher, J. Geophys. Research **55**, 437 (1950) and references therein.

[3] Morrison, Olbert, and Rossi, Phys. Rev. **94**, 440 (1954).